

# RSC Advances



This is an *Accepted Manuscript*, which has been through the Royal Society of Chemistry peer review process and has been accepted for publication.

*Accepted Manuscripts* are published online shortly after acceptance, before technical editing, formatting and proof reading. Using this free service, authors can make their results available to the community, in citable form, before we publish the edited article. This *Accepted Manuscript* will be replaced by the edited, formatted and paginated article as soon as this is available.

You can find more information about *Accepted Manuscripts* in the [Information for Authors](#).

Please note that technical editing may introduce minor changes to the text and/or graphics, which may alter content. The journal's standard [Terms & Conditions](#) and the [Ethical guidelines](#) still apply. In no event shall the Royal Society of Chemistry be held responsible for any errors or omissions in this *Accepted Manuscript* or any consequences arising from the use of any information it contains.

## Initial-stage oriented-attachment one-dimensional assembly of nanocrystals: Fundamental insight with a collision-recrystallization model

Yu Pan,<sup>1†</sup> Weiqiang Lv,<sup>1†</sup> Yinghua Niu,<sup>1</sup> Kechun Wen,<sup>1</sup> Xiaorong Hou,<sup>1</sup> Jianmin Gu,<sup>1</sup> Minda Zou,<sup>1</sup> Luhan Ye,<sup>1</sup> Wei Wang,<sup>2</sup> Kelvin HL Zhang,<sup>3\*</sup> Weidong He<sup>1,4,5\*</sup>

<sup>1</sup> School of Energy Science and Engineering, University of Electronic Science and Technology of China (UESTC), Chengdu 611731, PR China, <sup>2</sup> School of Materials Science and Engineering, Shenzhen Graduate School, Harbin Institute Technology, Shenzhen 518055, PR China, <sup>3</sup> Department of Materials Science & Metallurgy, University of Cambridge, 27 Charles Babbage Road, Cambridge, UK CB3 0FS, <sup>4</sup> Interdisciplinary Program in Materials Science, Vanderbilt University, Nashville, Tennessee 37234-0106, USA, <sup>5</sup> Vanderbilt Institute of Nanoscale Science and Engineering, Vanderbilt University, Nashville, Tennessee 37234-0106, USA. Correspondence and requests for materials should be addressed to K.H.L. Zhang and W. He. (Emails: hz256@cam.ac.uk, weidong.he@uestc.edu.cn and weidong.he@vanderbilt.edu). †These two authors contribute equally to this work.

### Abstract

Oriented attachment (OA) growth has been a promising method for the synthesis of one dimensional (1D) anisotropic nanocrystals (NCs). An unresolved fundamental issue is to understand the growth mechanism at the initial stage of an OA nanorod (NR) growth. In this report, a collision-recrystallization model is proposed to investigate the initial OA growth of NRs. The repulsive electrical double layer (EDL) interaction and the attractive van der Waals (vdW) interaction at the initial OA stage are derived by the accurate surface element integration (SEI) technique and the classical Hamaker equation, respectively. Our results show that the self-recrystallization of nanochains increases the collision activation energy of NPs dramatically as their surface potentials and Hamaker constants increase. Under a specific electrolyte concentration, the collision activation energy reaches the maximum, indicating that the growth rate of OA can be controlled by adjusting the electrolyte concentration.

### 1. Introduction

Oriented attachment (OA) has evolved to be a fundamental growth mechanism for nanocrystals (NCs).<sup>1</sup> In OA growth, nanoparticles (NPs) in a colloidal dispersion collide and attach together along a specific crystalline orientation. OA growth has exhibited great versatility and governed the synthesis of various functional materials and structures.<sup>2-5</sup> Compared to the traditional Ostwald ripening (OR) mechanism, OA exhibits unprecedented advantage in synthesizing anisotropic NRs of various materials.<sup>6-8</sup> In particular, the thermodynamics and kinetics of NR growth has been investigated extensively for the rational design of synthetic parameters in an OA growth.<sup>9-15</sup> The initial stage of an OA NR growth is of fundamental significance in the OA growth of NRs since it determines the following elongation of NRs. Several experimental observations *via* state-of-art *in-situ* techniques, such as *in-situ* high-resolution transmission electron microscopy (*in-situ* HR-TEM) have directly revealed the details of the initial OA assembly of NRs. For instance, Li *et al.* observed the dynamic collision and attachment process of two iron oxyhydroxide (FeOOH) NPs to form a dimer, and the subsequent collision of a primary NP with a dimer to form a tri-mer.<sup>16</sup> Such repeated collisions result in the formation of an N-mer (N is an integer), noted as a nanochain. Meanwhile, the collision interfaces of dimers or N-mers undergo continuous recrystallization and were completely eliminated near the completion of the OA growth. Similar process was also observed in the assembly of Pt<sub>3</sub>Fe NPs by Liao

*et al.*, showing the NR evolution from the initial nucleation in the molecular precursor solution to subsequent elongation of NRs *via* OA.<sup>17</sup> Such *in-situ* experiments demonstrate two primary processes at the initial stage of OA growth of NRs, which are collision and self-recrystallization. Collisions give rise to the elongation of NRs, while self-recrystallizations result in the elimination of collision interfaces and the smooth side-surfaces of NRs.

Although the initial processes have been explored experimentally, the driving forces associated with the collision and recrystallization at the initial stage of the anisotropic OA growth has remained rarely explored. A characteristic of this stage is the assembly between a primary NP and a dimer or a short nanochain. Modeling the initial stage of NR growth and investigating the interactions among different assembling NPs provide quantitative basis for studying the driving forces and the underlying thermodynamics and kinetics of an anisotropic OA growth. In this report, the interaction-driven collision/attachment at the initial stage of an OA nanorod growth is investigated for the first time. Two dominant inter-particle interactions in a colloidal system, the repulsive electrical double layer (EDL) and the attractive van der Waals (vdW) interaction, are evaluated quantitatively by an accurate surface element integration method (SEI) and classical Hamaker method, respectively. The effects of the major parameters on the growth of NRs at the initial stage *via* OA are presented, including precursor NP concentration, temperature, electrolyte concentration, surface potential of NPs and the Hamaker constant. Our work sheds new light on the rational design of synthetic parameters for anisotropic NCs with desirable physical properties.

## 2. Models and methodology

### 2.1 The collision- recrystallization model of 1D NR growth

A colloidal-self-recrystallization model is proposed to describe the initial stage of an OA NR growth. As shown in Figure 1(a), at the beginning two spherical NPs with a radius of  $R_0$  attach through a specific crystallographic orientation to form a dimer. A third NP then approaches the dimer with a separation distance of  $D$ , and two processes occur as shown in Figure 1(b). One process is the elongation of the dimer *via* the collision with a third precursor NP. The other process is the self-recrystallization of the dimer or nanochain. In the process of self-recrystallization, the grain boundary in the existing dimer formed in previous collision induces a decreased chemical potential. Therefore, the grain boundary merges gradually owing to the dissolution, diffusion and recrystallization of the exterior dimer atoms. As a result, the self-recrystallization of a dimer produces a smooth surface on the sides of the NPs to form an NR, as shown in Figures 1(b) and (c). During this process it is assumed that two geometric components exist in the dimer, which are the spherical segment and the cylindrical part. The cylindrical part is located between two spherical segments, as shown in Figure 1(b). As the self-crystallization proceeds, the thickness of the spherical segment ( $H_0$ ) decreases.  $H_0$  can therefore be used to measure the evolution of the self-crystallization. In addition, it is assumed that in the self-recrystallization process the dimer keeps a fixed volume and a constant radius  $R_0$  in the whole growth process. Based on the above assumptions, the length of the cylindrical part  $L_0$  in the growing dimer can be calculated through the geometric relation, as given in Eq. 1,

$$L_0 = \frac{4R_0^3 - 6H_0R_0^2 + 2H_0^3}{3R_0^2} \quad (1)$$

Notably, the length of NR  $L$  ( $= 2L_0$ ) is equal to  $8/3R_0$  as the self-recrystallization is completed ( $H_0$  decreases to 0). In our model, a  $R_0$  of 5 nm is used as a typical value, leading to an NR length  $L = 13.3$

nm at  $H_0 = 0$ , as illustrated in Figure 1(d).

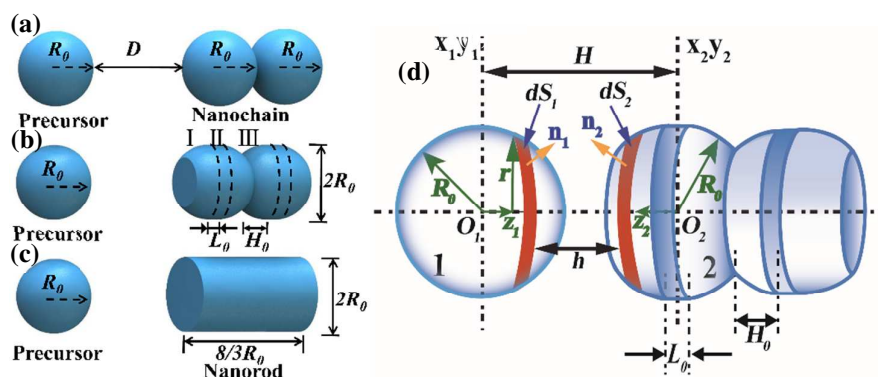


**Figure 1.** Configuration of a spherical precursor and a growing nanochain with three sequential growth states: (a) The initial state in which two precursors collide but the nanochain is not yet formed, and a third nanoparticle precursor approaches the nanochain; (b) The intermediate state in which the recrystallization of the nanochain occurs. The exterior atoms dissolve into solution, but diffuse and recrystallize on the interface near the collision point; (c) The final state in which the evolution of the nanochain is complete and an NR is formed; (d) A geometrical model of the intermediate state in (b) for SEI calculation of inter-particle interactions.

## 2.2 Dissolution, diffusion and recrystallization

The dissolution and recrystallization of the exterior atoms of an NP in an aqueous solution are subject to the surface energy and the surface curvature based on thermodynamics. Gibbs-Thompson relation provides the correlation between the solubility of exterior NP atoms and their relative chemical potential  $\Delta\mu$ , as given in Eq. 2,<sup>18</sup>

$$S_c = S_\infty \exp\left(\frac{\Delta\mu}{k_B T}\right) \quad (2)$$

where  $S_c$  is the solubility of atoms on curved surfaces,  $S_\infty$  represents the solubility of atoms on an infinite flat surface,  $k_B$  is the Boltzmann constant and  $T$  is temperature.  $\Delta\mu$  is the relative chemical potential of the exterior atoms on the NP, corresponding to an infinite flat surface.  $\Delta\mu$  can be described by the Young-Laplace equation, as shown in Eq. 3,<sup>18</sup>

$$\Delta\mu = \frac{2\gamma\Omega}{R} \quad (3)$$

where  $\gamma$  is the surface energy of the exterior atoms,  $\Omega$  is the atomic volume, and  $R$  is the curvature radius. Thus, the solubility of exterior atoms can be expressed as a function of the surface energy and the curvature radius according to Eqs. 2 and 3. Since only the site of grain boundary has negative curvature radius, showing lower chemical potential compared with other sites, atoms from other facets, for instance, the end facets of the nanochain, dissolve and are thermodynamically favored to move to the nearby joint before the grain boundary is eliminated. For convenience, it is assumed as a hypothetical final state of recrystallization in this study that the end facets transform gradually to flat surfaces as OA growth proceeds. In fact, the recrystallization ends before  $H_0$  decreases to 0.

## 2.3 Theoretical calculation of inter-particle interactions

The interactions between a precursor NP and a growing nanochain of continuous self-recrystallization typically include a repulsive EDL interaction and an attractive vdW interaction.<sup>13</sup>

Accurate calculation of the two interactions is conducted with surface element integration (SEI) methods.

### 2.3.1 EDL interaction

NPs submerged in an electrolyte solution absorb potential-determining ions onto the NP surface by chemical binding, and then generate a compact charging layer, noted as the Stern layer. These anchored ions continue to attract counter ions in the electrolyte by electrostatic forces and form a diffusion layer surrounding the Stern layer. As a consequence, an electrical double layer structure is established, which ensures the stability of the colloidal dispersion by providing a mutually repulsive surface charge to prevent colloidal particles from aggregating. Due to the existence of EDL around NPs, the repulsive EDL interactions between NPs during the OA growth must be taken into consideration. On the basis of the Gouy-Chapman model and the superposition approximation, the electrical double layer interaction energy per unit area between two infinite flat surfaces is given in Eq. 4,<sup>19</sup>

$$E(h) = 64k_B T n_\infty \kappa^{-1} \Upsilon_0^2 \exp(-\kappa h) \quad (4)$$

where  $n_\infty$  is the number of indifferent solute ions per cubic meter far from the surface of NPs,  $h$  is the separation distance between two infinite flat surfaces, and  $\kappa^{-1}$  is the Debye-Hückel length. The parameter  $\Upsilon_0$  is defined in Eq. 5,

$$\Upsilon_0 = \frac{\exp(z e \psi_0 / 2k_B T) - 1}{\exp(z e \psi_0 / 2k_B T) + 1} \quad (5)$$

where  $\psi_0$  is the surface potential of the NPs which distributes uniformly on the NPs' surface,  $z$  is the valence number of the indifferent solute ions, and  $e$  is the elementary charge.  $\kappa^{-1}$  is a function of  $n_\infty$  and  $T$ , as given in Eq. 6,<sup>19</sup>

$$\kappa^{-1} = \left( \frac{e^2}{\epsilon k_B T} \sum_i z_i n_i \right)^{-1/2} \quad (6)$$

where  $\epsilon$  represents the absolute permittivity of the solution.  $\kappa^{-1}$  has the unit of length and is viewed as EDL thickness.

Due to the complexity to directly solve the potential of the curved EDL from the Poisson-Boltzmann equation, Derjaguin Approximation (DA) is typically adopted to obtain the approximate solution by dividing the spherical surface into a series of circular planar faces. However, this conventional method neglects the effect of NP surface curvature and orientation giving rise to the overestimation of interactions for small NPs in dilute solution. The results is relatively accurate only if the separation between two flat surfaces is negligible compared to the size of NPs ( $h^2/R_0^2 \ll 1$ ) and the radius of NPs is 10 times larger than the EDL thickness ( $\kappa R_0 > 10$ ).<sup>19,20</sup> To overcome these limitations, we use the SEI technique, which is preferable for curved surfaces with constant potential and provides more accurate results by considering the orientation of the approximated planar faces.<sup>20</sup> The EDL interaction between two curved surfaces based on the SEI technique is expressed in Eq. 7,<sup>21</sup>

$$U_{EDL} = \int_{S_1} dU = \int_{A_1} \mathbf{n}_2 \cdot \mathbf{k}_2 \frac{\mathbf{n}_1 \cdot \mathbf{k}_1}{|\mathbf{n}_1 \cdot \mathbf{k}_1|} E(h) dA_1 \quad (7)$$

where  $A_1$  is the  $xy$ -plane projected area of the actual surface of particle 1,  $S_1$ ,  $dA_1$  is the  $xy$ -plane projected area of the differential area elements on the surfaces of particle 1,  $dS_1$ .  $\mathbf{n}_1$  and  $\mathbf{n}_2$  are the unit normal vectors outward the approaching differential surface elements, respectively,  $\mathbf{k}_1$  and  $\mathbf{k}_2$  are the

unit vectors parallel to z axes in their respective coordinate system on each NP. Here  $h$  is the separation along z axis between  $dS_1$  and  $dS_2$ . All these parameters are shown in Figure 1(f). EDL interaction is dependent on the shape of NPs according to Eq. 7. In our model, the EDL interaction between an approaching precursor NP and a growing nanochain is considered as the sum of a series of interactions among different surface pairs. The interaction of each pair can be obtained by numerical integration. The detailed theoretical derivation is provided in the Supporting Information.

### 2.3.2 vdW interaction

In contrast to the repulsive EDL interaction, the other dominant interaction among the NPs is the attractive van der Waals interaction. Hamaker has given the expression of the vdW interaction energy between two macroscopic bodies, as shown in Eq. 8,<sup>22</sup>

$$U_{vdW} = -\int_{V_1} dV_1 \int_{V_2} dV_2 \frac{q^2 \lambda}{r^6} \quad (8)$$

where  $dV_1$  and  $dV_2$  are the volume elements of macroscopic particles,  $V_1$  and  $V_2$  are the particle volumes,  $q$  represents the atom density of particles,  $\lambda$  is the London-van der Waals constant, and  $r$  represents the distance between  $dV_1$  and  $dV_2$ . In addition, the constant  $\pi^2 q^2 \lambda$  is often substituted by  $A$ , the Hamaker constant. In this study,  $A$  is assumed to be  $\sim 10^{-19}$  J, which is on the same order of Hamaker constants of a variety of metals and metal oxides. Similar to the calculation of EDL interactions, the total vdW interaction is divided into the interactions between separated volumes. The interaction of each pair of volumes can be calculated by numerical integration. The detailed derivation is shown in the Supporting Information. By taking the overall effect of two interactions into account, the total interaction energy is given in Eq. 9.

$$U_{tot} = U_{EDL} + U_{vdW} \quad (9)$$

EDL interaction increases exponentially while the vdW interaction increases inversely proportional to the sixth power of distance as separation distance decreases. If the overall interaction energy of the system is plotted as a function of distance between NPs, it is seen that there exists a total potential energy maximum as the spherical precursor approaches the growing nanochain as shown in Figure 2. This maximum is defined as the activation energy  $E_a$  of OA growth since it is the energy barrier for the formation of a nanochain from NPs. Moreover, the separation between the precursor and the nanochain at  $E_a$  is defined as the critical separation  $d_c$ . Based on activation energy  $E_a$ , the OA growth rate can be evaluated according to the Arrhenius equation, as given in Eq. 10,<sup>23</sup>

$$k = Z \rho \exp\left(\frac{-E_a}{k_B T}\right) \quad (10)$$

where  $k$  is the rate constant of nanochain formation,  $\rho$  is the steric factor, and  $Z$  is the collision frequency. The lower the activation energy is, the more likely an effective collision between NPs occurs and the faster the OA growth is.

## 3. Results and Discussion

At the initial stage of an OA NR growth, the morphology of the as-synthesized nanostructure and the growth rate are determined largely by synthetic parameters including the concentration of precursor NPs, temperature, electrolyte additives and ligands. The focus of this report is to investigate how these parameters affect the OA growth from an energetic standpoint by employing the aforementioned collision-recrystallization model.

### 3.1 The effect of precursor concentration

The effect of the concentration of precursor NPs on the inter-particle interaction between an NP and a self-recrystallizing nanochain with different  $H_0$  is investigated first. The concentration of precursor NPs in the solution is considered to be inversely proportional to the mean inter-particle separation distance ( $D$ ), and  $D$  is then employed in the calculation instead of the concentration. The plots of EDL, vdW and total interaction *versus*  $D$  are shown in Figure 2. As shown in Figure 2(a), EDL interaction increases exponentially as  $D$  decreases regardless of  $H_0$ . This means that as the concentration of precursor NPs increases, the average inter-particle repulsive EDL interaction increases. On the other hand, in a colloidal system with a specific precursor concentration where the average inter-particle separation  $D$  is fixed, EDL interaction increases as  $H_0$  decreases, indicating that a nanochain with a higher extent of self-recrystallization experiences a larger EDL repulsive interaction. Figure 2(b) shows inter-particle vdW interactions *versus*  $D$ . vdW varies little once  $D$  is larger than 5 nm. However, as  $D$  is below 5 nm, the attractive vdW increases significantly as  $D$  decreases for nanochains with any  $H_0$ . In addition, vdW increases as  $H_0$  decreases at fixed  $D$ . For example, the inset of Figure 2(b) shows that the nanochain without any self-recrystallization ( $H_0 = 5$  nm) experiences smaller vdW forces with a nearby NP compared to a nanochain with a small extent of self-recrystallization ( $H_0 = 4$  nm). However, the vdW interaction varies little as  $H_0$  further decreases below 4 nm. Therefore, there exists an optimized recrystallization state of nanochains, at which the attractive vdW driving force for OA assembly reaches the maximum. The total interaction between a nanochain and an NP is shown in Figure 2(c) by considering both repulsive EDL and attractive vdW interactions. The interaction energy maximum  $E_a$ , defined as the collision energy barrier, increases as  $H_0$  decreases, suggesting that the OA growth of nanochains experiences increased energy barrier as self-recrystallization proceeds. The critical separation distance  $d_c$ , defined as the separation where the energy maximum is reached, increases as  $H_0$  decreases. These results illustrate that a lower precursor concentration is beneficial for the OA growth of nanochains with either partial or complete self-recrystallization, whereas a higher concentration of precursors is required for the fast OA growth of nanochains without self-recrystallization. It is noted that as particle size increases, only the absolute values such as collision energy barrier and critical separation vary. The main conclusions made in this study are not affected by particle size.

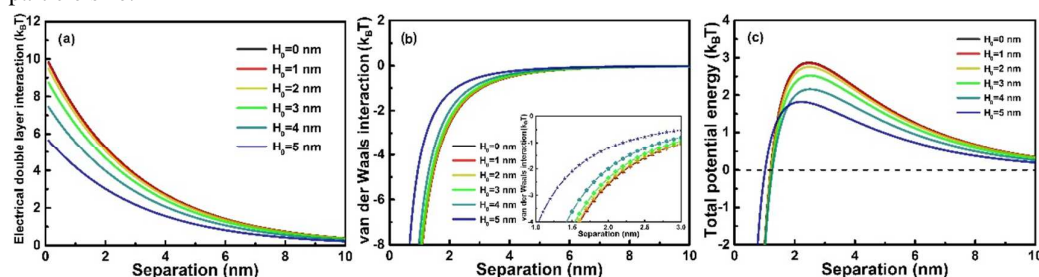


**Figure 2.** Plots of inter-particle (a) EDL interaction, (b) vdW interaction and (c) total interaction interactions *versus* surface-to-surface separation  $d$  between a spherical precursor NP and a growing nanochain. The inset in (b) shows the magnified plot in the range of  $D$  between 1.0 nm and 3.0 nm. The relative permittivity of the solution  $\epsilon = 78.3$ , electrolyte concentration  $M = 0.01$  mol/L, surface potential of  $\psi_0 = 50$  mV, Hamaker constant  $A = 10^{-19}$  J and  $T = 298$  K.

### 3.2 The effect of temperature

The effect of temperature on the self-recrystallization and collision is shown in Figure 3. Figure 3(a) shows  $E_a$  variation with  $H_0$  at different temperatures.  $E_a$  decreases as  $H_0$  increases, and such a decrease becomes abrupt as  $H_0 > 3$ . At a fixed  $H_0$ ,  $E_a$  decreases as the temperature increases. The changes of  $E_a$

at different temperatures become larger as  $H_0$  is smaller than 2 nm, which indicates that the collision process is accelerated as temperature increases. This effect is more prominent at temperatures below 328 K, as evidenced by steeper curve. The critical distance *versus*  $H_0$  at different temperatures is plotted in Figure 3(b).  $d_c$  increases initially as  $H_0$  decreases but becomes stable at smaller  $H_0$ . As temperature increases,  $d_c$  increases, indicating that a more dilute precursor concentration can be used for the OA growth of 1D nanochain/NR. It should be noted that the effects of temperature on  $E_a$  and  $d_c$  in the collision and self-recrystallization process at the initial OA stage arise from the different responses of EDL and vdW to the temperature change; EDL decreases significantly as temperature increases, while vdW does not change as much with temperature. According to the Eq. 5, the EDL interaction is a function of temperature. Temperature affects EDL interaction *via* the surface charge density of the nanoparticles,  $\sigma^*$ , and the thickness of EDL,  $\kappa^{-1}$ . Eq. 11 provides an approximate correlation between the charge density on the nanoparticles and the temperature of the solution.<sup>19</sup>

$$\sigma^* = (2n_\infty \varepsilon k_B T)^{1/2} [\exp(ze\psi_0 / 2k_B T) - \exp(-ze\psi_0 / 2k_B T)] \quad (11)$$

Moreover, the surface potential of the nanoparticles is determined by the Nernst equation as shown in Eq. 12,<sup>19</sup>

$$\psi_0 = \frac{k_B T}{xe} \ln\left(\frac{c}{c_{zp}}\right) \quad (12)$$

where  $x$  is the valence number of the potential-determining ions  $M^{x+}$ ,  $c$  is the concentration of the potential-determining ions  $M^{x+}$ , and  $c_{zp}$  represents a concentration point of the potential-determining ions corresponding to the nanoparticle surface with zero charge, abbreviated as p.z.c. (point of zero charge). Hence, the nanoparticle surface is positively charged as  $c$  is larger than p.z.c. Combining Eqs. 11 and 12, it can be deduced that  $\sigma^*$  decreases as p.z.c. increases. p.z.c. is found to increase with increasing temperature.<sup>24, 25</sup> Thus  $\sigma^*$  decreases as temperature increases. In addition, according to Eq. 6, increasing temperature compresses the EDL thickness, since the product  $\varepsilon T$  decreases with increasing temperature. Thus, the coverage of the EDL shrinks as temperature increases and the EDL interaction attenuates rapidly as the separation between two nanoparticles is larger than  $\kappa^{-1}$ . Therefore,  $U_{EDL}/k_B T$  decreases as temperature increases.

vdW interaction almost does not change as temperature changes according to Eq. 8, since the Hamaker constant or the atom density  $q$  of nanoparticles is reduced subtly with increasing temperature. In addition, temperature cannot influence molecular instantaneous dipoles in nanoparticles, as generated by the fluctuation of electron cloud. Therefore, the influence of temperature on vdW interaction is negligible. The variation of total inter-particle interaction with temperature mainly arises from the variation of EDL interaction. In conclusion of this section, increasing temperature decreases largely the collision energy barrier regardless of self-recrystallization, increases the critical distance, and thus facilitates an increased OA growth rate, especially for a dilute precursor dispersion.

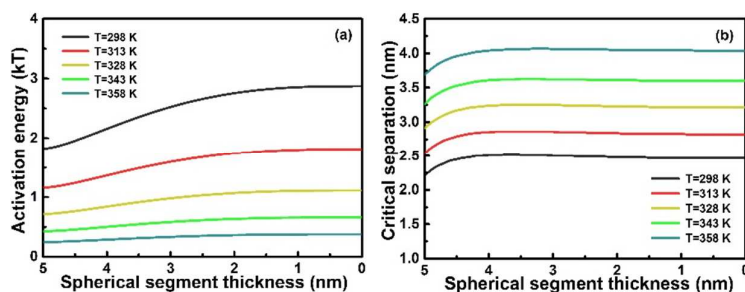


**Figure 3.** Plots of (a) activation energy and (b) critical separation *versus* the spherical segment thickness of a growing nanochain at different temperatures. The electrolyte concentration is kept at  $M = 0.01$  mol/L, surface potential at  $\psi_0 = 50$  mV and Hamaker constant at  $A = 10^{-19}$  J.

### 3.3 The effect of electrolyte concentration

Electrolyte concentration is also an important factor in the OA growth of NRs.<sup>26</sup> Varying electrolyte concentration typically affects EDL interactions by varying Debye length and surface potential on the surface of NPs. Figure 4(a) shows that at any give  $H_0$  the activation energy  $E_a$  increases as the electrolyte concentration increases until a peak is reached at  $\sim 0.01$  mol/L. According to Eq. 4, EDL interaction is a function of electrolyte concentration.  $\sigma^*$  increases as electrolyte concentration increases according to Eqs. 11 and 12, and the electrostatic repulsion between precursors and nanochains thus increases considerably, leading to the elevation of  $E_a$ . However, the Debye–Hückel length  $\kappa^{-1}$  decreases with increasing electrolyte concentration according to Eq. 6, which indicates that more indifferent counter ions move close to nanoparticle surfaces and screen the EDL force. Therefore, there must exist a critical concentration, which is  $\sim 0.01$  mol/L with the parameters employed in this study. Below the critical concentration, EDL interaction increases with increasing electrolyte concentration due to increasing surface charge. Above the critical concentration, EDL interaction decreases due to the screen effect. The critical electrolyte concentration is correlated to the temperature, surface potential and nanoparticle precursor concentration since EDL interaction is affected largely by these factors. In a synthetic experiment, to minimize the  $E_a$  of an OA growth, the critical electrolyte concentration should be avoided. Figure 4(b) shows that  $d_c$  decreases rapidly as the electrolyte concentration increases below the critical value and above the critical value, such a decrease becomes gradual. For instance, for an NP with a nanochain of  $H_0 = 5$  nm, as shown in the inset graph  $d_c$  decreases from  $\sim 3.8$  nm at 0.002 mol/L to  $\sim 2.2$  nm at 0.01 mol/L, but only decreases from  $\sim 2.2$  nm at 0.01 mol/L to 1.7 nm at 0.04 mol/L. This suggests that increasing electrolyte concentration facilitates the controlled OA growth in a media with higher concentration of precursor nanoparticles. For nanochains even with a small portion of self-recrystallization,  $d_c$  increases notably, especially as the electrolyte concentration is above 0.01 mol/L. Such results indicate that the stability of the colloidal dispersion increases as the self-crystallization proceeds in an OA growth.

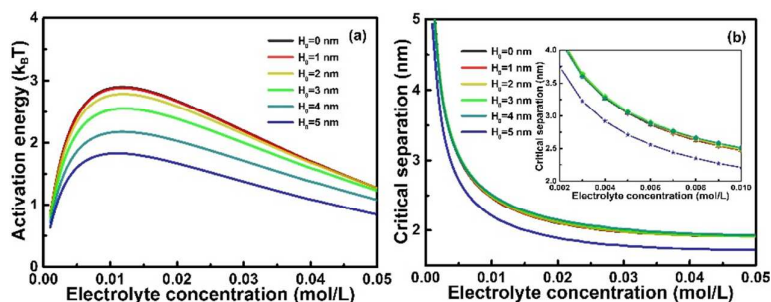


**Figure 4** Plots of (a) activation energy and (b) critical separation *versus* electrolyte concentration of the solution at different spherical segment thicknesses  $H_0$  of a growing nanochain. The relative permittivity of solution  $\epsilon = 78.3$ , surface potential  $\psi_0 = 50$  mV, Hamaker constant  $A = 10^{-19}$  J and  $T = 298$  K.

### 3.4 The effect of NP surface potential

Surface potential of NPs in a colloidal dispersion, which is adjustable by manipulation of the dispersion pH and temperature, is another factor influencing the growth rate of OA.<sup>27, 28</sup> Unlike zeta potential, surface potential cannot be measured directly, but it can be easily determined with Eq. 12. Figure 5 shows the plots of  $E_a$  and  $d_c$  *versus* surface potential. As shown in Figure 5(a),  $E_a$  increases as

surface potential increases, and this increase become predominant as  $\psi_0 > 30$  mV, a value believed typically to be the minimum to keep a stable colloidal dispersion.<sup>19</sup> For nanochains of different  $H_0$ ,  $E_a$  increases as  $H_0$  decreases at fixed surface potential. At higher surface potentials, the increase of  $E_a$  with  $H_0$  becomes more obvious, indicating that at lower surface energy, the self-recrystallization of nanochain has less effect on the collision process compared with higher surface potentials. Figure 5(b) shows that  $d_c$  decreases as surface potential increases, and  $d_c$  varies little as  $H_0$  varies. As shown in the inset graph of Figure 5(b), only  $\sim 0.5$  nm difference in  $d_c$  is found as  $H_0$  changes from 5 nm to 4 nm and  $d_c$  keeps almost constant as  $H_0$  decreases further. The result indicates that the dispersion stability increases with increasing surface potential, and a higher  $E_a$  should be overcome for inter-particle collisions as the self-crystallization proceeds in an OA growth.

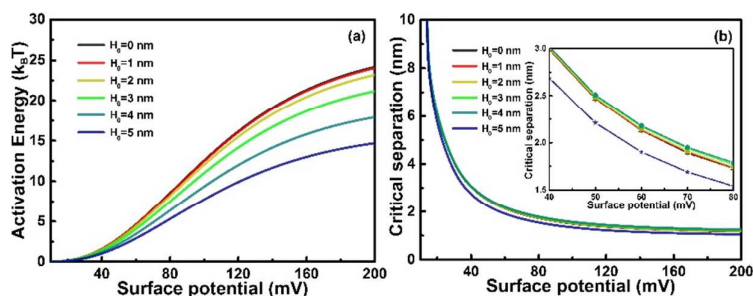


**Figure 5.** Plots of (a) activation energy and (b) critical separation versus surface potential at different spherical segment thicknesses of a growing nanochain. Inset in (b): the magnification graph of (b) as surface potential locates in the range of 40–80 mV. The relative permittivity of solution  $\epsilon = 78.3$ , electrolyte concentration  $M = 0.01$  mol/L, Hamaker constant  $A = 10^{-19}$  J and  $T = 298$  K.

### 3.5 The effect of Hamaker constant

Hamaker constant ( $A$ ) is correlated directly with the inter-particle vdW according to Eq.8. The investigation of the effect of Hamaker constant on  $E_a$  and  $d_c$  facilitates our understanding on the interactions of NPs of a specific material. As shown in Figure 6,  $E_a$  decreases monotonically as  $A$  increases. At fixed  $A$ ,  $E_a$  increases as  $H_0$  decreases, and such an increase becomes subtle as  $A$  increases. Figure 6(b) shows that  $d_c$  increases as  $A$  increases. At a specific  $A$ ,  $d_c$  for nanochains of  $H_0 = 5$  nm is  $\sim 0.25$  nm for  $H_0$  in the range of 0–4 nm, as shown in the inset of Figure 6(b). The result indicates that nanochains with a small portion of self-recrystallizations and with a larger  $A$  experience low  $E_a$  and relatively small  $d_c$  and, thus, are featured with a high rate of OA growth. In addition, solvent also influences the Hamaker constant, and thus inter-particle vdW interaction. Considering that nanoparticles interact with solvent molecules, The Hamaker constant  $A$  is typically developed into the following form as shown in Eq. 13,<sup>22</sup>

$$A = \pi^2 (q_1^2 \lambda_{11} + q_0^2 \lambda_{00} - 2q_1 q_0 \lambda_{01}) \quad (13)$$

where the subscripts 1 and 0 represent nanoparticle and solvent, respectively,  $q_1$  and  $q_0$  are the atomic densities of nanoparticle and solvent, respectively.  $\lambda_{11}$ ,  $\lambda_{00}$  and  $\lambda_{01}$  are London-van der Waals constants for the pairs of the substances noted by the subscripts. The London-van der Waals constant  $\lambda$  is expressed by Eq. 14,<sup>22</sup>

$$\lambda_{kl} = \frac{3}{2} \alpha_k \alpha_l \frac{I_k I_l}{I_k + I_l} \quad (14)$$

where  $\alpha_k$  and  $\alpha_l$  represent the dipole polarizabilities of materials  $k$  and  $l$ , respectively.  $I_k$  and  $I_l$  are the

first ionization energies of materials  $k$  and  $l$ , respectively. Based on Eqs. 13 and 14, nanoparticles prefer to attach at a high atom density plane with a strong dipole polarizability and a sufficient ionization energy in a low atom density solvent, such as ethanol solution. For metal nanoparticles such as gold nanoparticles, the Hamaker constant of which varies from  $16.2 \times 10^{-20}$  J to  $45.5 \times 10^{-20}$  J, oriented aggregation is more likely to occur compared with oxide nanoparticles of Hamaker constants from  $10.5 \times 10^{-20}$  J to  $15.5 \times 10^{-20}$  J.<sup>29</sup>

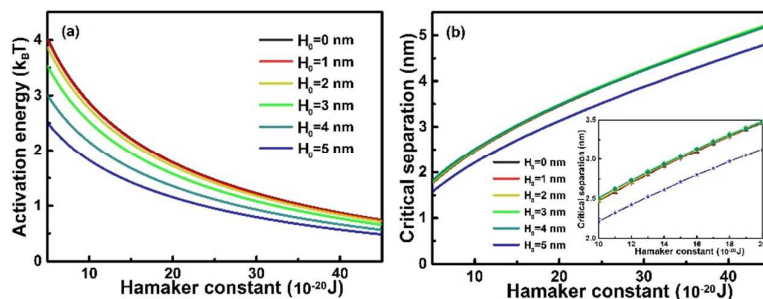


**Figure 6.** Plots of (a) activation energy and (b) critical separation *versus* Hamaker constant at different spherical segment thicknesses of a growing nanochain. Inset: the magnification of (b) in the Hamaker range of  $1 \times 10^{-19}$ – $2 \times 10^{-19}$  J. The relative permittivity of solution  $\epsilon = 78.3$ , electrolyte concentration  $M = 0.01$  mol/L, surface potential  $\psi_0 = 50$  mV and  $T = 298$  K.

In addition, attention should also be paid to the effect of solvents. Organic solvents show typically much smaller dielectric constants than that of water. Therefore, with organic solvents the EDL thickness becomes thinner according to Eq. 6, and EDL interaction becomes smaller according to Eq. 4. Due to the decrease of EDL repulsive interaction, NPs trend to aggregate. For the controlled OA growth of well-defined nanostructures, organic solvents with larger viscosities should be used to suppress the Brownian motion and decrease the OA growth rate. Surfactants such as long-chain alkyl-amine/acid can also be used to induce steric effect. Despite the simplicity of the numerical models in this study to quantitatively describe the initial stage of OA growth by EDL and vdW interactions, the collision and self-recrystallization processes of NPs are influenced frequently by surface ligands, the crystallographic anisotropy, and the motion and elimination of defects such as dislocations at grain boundaries. For instance, surface ligands can induce steric force as two NPs approach. Surface polarity due to different materials and irregular-shape induced unbalanced electron density influence largely the surface charge. Charged ligands like ionic surfactants also alter the surface charge distribution of NPs and influence the EDL interaction dramatically. All these factors are not included in our numerical models. Further studies should be focused on these factors in detail from mesoscopic and atomic levels.

#### 4. Conclusions

A collision-recrystallization model has been proposed to study the initial stage of NR formation *via* the OA mechanism. Based on our model, the theoretical expressions of the total interaction energy including the repulsive EDL interaction and the attractive vdW interaction are derived by the accurate SEI technique and the classical Hamaker equation, respectively. The EDL, vdW and total energy between an NP and a nanochain of continuous self-recrystallization are then calculated by investigating both the parameters of precursor NPs, including precursor concentration, precursor morphology (or the extent of self-recrystallization of a nanochain), surface potential, Hamaker constant, and the parameters of solutions, such as electrolyte concentration and temperature. The results show that the collision activation energy of NPs in the OA growth increases dramatically with the evolution of

self-recrystallization, and such increase is more pronounced as NP surface potential and Hamaker constant increase. OA growth is favored in the colloidal dispersion with a high primary precursor concentration, a high temperature and a moderate electrolyte concentration. In addition, the OA growth rate can be controlled by adjusting the electrolyte concentration in the dispersion system. With a specific electrolyte concentration, the collision activation energy reaches the maximum. Our work facilitates the theoretical understanding on the role of interactions with the initial morphology evolution of nanocrystals in the OA growth.

### Acknowledgements

The work is supported in part by the UESTC new faculty startup fund, by the National Natural Science Foundation (grant no. 21403031 and 11402069) and by Shenzhen Peacock Technological Innovation Program (Grant No. KQCX20140521144102503).

### References

- Penn, R. L.; Banfield, J. F. *Science* **1998**, *281*, 969.
- Zhang, Q.; Liu, S. J.; Yu, S.H. *J. Mater. Chem.* **2009**, *19*, 191.
- Yu, X. F.; Wang, D. S.; Peng, Q.; Li, Y. D. *Chem-Eur. J.* **2013**, *19*, 233.
- Zeng, C. Y.; Zhang, W. X.; Ding, S. X.; Yang, Z. H.; Zeng, H.; Li, Z. C. *CrystEngComm* **2013**, *15*, 5127.
- Song, H.; Lee, K. H.; Jeong, H.; Um, S. H.; Han, G. S.; Jung, H. S.; Jung, G. Y. *Nanoscale* **2013**, *5*, 1188.
- Liang, H. Y.; Zhao, H. G.; Rossouw, D.; Wang, W. Z.; Xu, H. X.; Botton, G. A.; Ma, D. L. *Chem. Mater.* **2012**, *24*, 2339.
- Kim, M. S.; Sung, Y. M. *CrystEngComm* **2012**, *14*, 1948.
- Yu, F.; Xu, X.; Baddeley, C. J.; et al. *CrystEngComm* **2014**, *16*, 1714-1723.
- Spagnoli, D.; Banfield, J. F.; Parker, S. C. *J. Phys. Chem. C* **2008**, *112*(38), 14731-14736.
- Zhang H.; Banfield, J. F.; *CrystEngComm* **2014**, *16*(8), 1568-1578.
- Raju, M.; van Duin, A. C. T.; Fichthorn, K. A. *Nano Lett.* **2014**, *14*(4), 1836-1842.
- He, W.; Lin, J.; Wang, B.; Tuo, S.; Pantelides, S. T.; Dickerson, J. H. *Phys. Chem. Chem. Phys.* **2012**, *14*, 4548.
- Lv, W.; He, W.; Wang, X.; Niu, Y.; Cao, H.; Dickerson, J. H.; Wang, Z. *Nanoscale* **2014**, *6*, 2531.
- He, W.; Lin, J.; Lin, X.; et al. *Analyst* **2012**, *137*(21), 4917-4920.
- He, W. and Dickerson, J. H., *Appl. Phys. Lett.* **2011**, *98*, 081914.
- Li, D.; Nielsen, M. H.; Lee, J. R.; Frandsen, C.; Banfield, J. F.; De Yoreo, J. J. *Science* **2012**, *336*, 1014.
- Liao, H. G.; Cui, L.; Whitlam, S.; and Zheng, H.; *Science* **2012**, *336*, 1011-1014.
- Cao, G. *Nanostructures and Nanomaterials: Synthesis, Properties and Applications*; World Scientific, **2004**, ISBN 1-86094-415-9
- Hiemenz, P. C.; Rajagopalan, R. *Principles of Colloid and Surface Chemistry, revised and expanded*; CRC Press, **1997**; Vol. 14.
- Bhattacharjee, S.; Elimelech, M. *J. Colloid Interf. Sci.* **1997**, *193*, 273.
- Bhattacharjee, S.; Elimelech, M.; Borkovec, M. *Croat. Chem. Acta* **1998**, *71*, 883.
- Hamaker, H. *physica* **1937**, *4*, 1058.
- Leite, E. R.; Ribeiro, C. *Crystallization and growth of colloidal nanocrystals*; Springer, **2011**.
- Berube, Y.; de Bruyn, P. L. *J. Colloid Interf. Sci.* **1968**, *27*, 305.
- Lopez Valdivieso, A.; Reyes Bahena, J.; Song, S.; Herrera Urbina, R. *J. Colloid Interf. Sci.* **2006**, *298*, 1.
- Burrows, N. D.; Hale, C. R. H.; Penn R. L.; *Cryst. Growth Des.*, **2012**, *12*(10), 4787-4797.
- Dunphy Guzman K. A.; Finnegan M. P.; Banfield J. F.; *Environ. Sci. Technol.* **2006**, *40*, 7688-7693.
- Yin, S.; Huang, F.; Zhang, J.; Zheng, J.; Lin, Z. *J. Phys. Chem. C*, **2011**, *115*(21), 10357-10364.
- Pierre, A. C. *Introduction to Sol-Gel Processing*; Kluwer, Norwell, MA, **1998**.